

## RESEARCH ARTICLE

# Universal principles of membrane protein assembly, composition and evolution

Alan J. Situ<sup>1</sup>, Tobias S. Ulmer<sup>1,2\*</sup>

**1** Department of Physiology and Neuroscience, Keck School of Medicine, University of Southern California, Los Angeles, CA, United States of America, **2** Department of Biochemistry and Molecular Medicine, Keck School of Medicine, University of Southern California, Los Angeles, CA, United States of America

\* [tulmer@usc.edu](mailto:tulmer@usc.edu)



## OPEN ACCESS

**Citation:** Situ AJ, Ulmer TS (2019) Universal principles of membrane protein assembly, composition and evolution. PLoS ONE 14(8): e0221372. <https://doi.org/10.1371/journal.pone.0221372>

**Editor:** Surajit Bhattacharjya, Nanyang Technological University, SINGAPORE

**Received:** June 4, 2019

**Accepted:** August 5, 2019

**Published:** August 15, 2019

**Copyright:** © 2019 Situ, Ulmer. This is an open access article distributed under the terms of the [Creative Commons Attribution License](https://creativecommons.org/licenses/by/4.0/), which permits unrestricted use, distribution, and reproduction in any medium, provided the original author and source are credited.

**Data Availability Statement:** All relevant data are within the manuscript and its Supporting Information files.

**Funding:** This work received funding from American Heart Association Grant #18TPA34170481 and National Institutes of Health Grant R03AG063284 to TSU. The funders had no role in study design, data collection and analysis, decision to publish, or preparation of the manuscript.

**Competing interests:** The authors have declared that no competing interests exist.

## Abstract

Structural diversity in  $\alpha$ -helical membrane proteins (MP) arises from variations in helix-helix crossings and contacts that may bias amino acid usage. Here, we reveal systematic changes in transmembrane amino acid frequencies ( $f$ ) as a function of the number of helices ( $n$ ). For eukarya, breaks in  $f(n)$  trends of packing (Ala, Gly and Pro), polar, and hydrophobic residues identify different MP assembly principles for  $2 \leq n \leq 7$ ,  $8 \leq n \leq 12$  and  $n \geq 13$ . In bacteria, the first  $f$  break already occurs after  $n = 6$  in correlation to an earlier  $n$  peak in MP size distribution and dominance of packing over polar interactions. In contrast to the later  $n$  brackets, the integration levels of helix bundles continuously increased in the first, most populous brackets indicating the formation of single structural units (domains). The larger first bracket of eukarya relates to a balance of polar and packing interactions that enlarges helix-helix combinatorial possibilities (MP diversity). Between the evolutionary old, packing and new, polar residues  $f$  anti-correlations extend over all biological taxa, broadly ordering them according to evolutionary history and allowing  $f$  estimates for the earliest forms of life. Next to evolutionary history, the amino acid composition of MP is determined by size ( $n$ ), proteome diversity, and effective amino acid cost.

## Introduction

Membrane proteins (MP), defined as traversing the lipid bilayer at least once, mediate the exchange of metabolites, ions, and information between different cellular compartments. This puts MP in control of key physiological and pathological processes as is evident from the large number of drugs that target MP [1]. Genomes typically contain 20–30% proteins that populate the membrane [2]. Despite their high biological and medical significance, MP are poorly understood especially on a structural level when compared to water-soluble proteins. As proteins traverse the membrane they need to navigate the aqueous cytosol, the chemically complex lipid headgroups, and the hydrophobic lipid hydrocarbon tails [3]. Moreover, arising from lipid diversity and membrane asymmetry [4, 5], this environment is cell-type specific and anisotropic along the membrane normal. Difficulties to reproduce functional lipid environments *in vitro* contribute to the relatively slow progress of MP structural biology and present value in seeking complementary approaches.

MP traverse the lipid bilayer either as  $\alpha$ -helices or  $\beta$ -sheets. To fulfill hydrogen bonding requirements when traversing the membrane core,  $\beta$ -sheets must form closed barrel structures [6, 7]. In contrast, intrahelical hydrogen bonding allows single  $\alpha$ -helices to traverse the membrane. The larger ensuing freedom in helix-helix compared to sheet-sheet orientations invariably allows a larger structural diversity, which could explain the nearly exclusive use of  $\alpha$ -helical MP in all membranes with the exception of bacterial outer membranes. The success of  $\beta$ -barrels in outer membranes may relate to their relatively high aqueous solubility in the unfolded state and robust folding pathway [6]. However, the dominance of  $\alpha$ -helical folds prompts us to exclusively focus on  $\alpha$ -helical MP.

In the course of evolution, as organisms developed increasingly complex functional needs, the repertoire of MP structures must have expanded to implement these functions. Structural diversity in mainly parallel TM helix bundles invariably relates to helix count and length, the number and location of helix-helix crossings, and the chemical nature of helix-helix interactions. Certain aspects of these properties can be quantified from the amino acid (AA) sequence of MP. The number of TM helices, termed  $n$ , and helix length can be predicted computationally [2, 8]. The number and location of helix-helix crossings often correlates with Pro-mediated helix kinks [9–11]. Helix-helix interactions regularly utilize recurring motifs centering, for example, on glycine packing or polar interactions [9, 12–14]. Such properties appear difficult to interpret for individual MP. We therefore analyzed the frequencies of all TM AA for entire biological taxa as a function of  $n$ , which allowed not only insight into universal assembly principles of MP but also into the drivers of MP diversity, AA composition, and evolution.

## Results and discussion

### The size distribution of MP peaks earlier in bacteria than eukarya

To achieve an even coverage of TM sequence space at a resolution that is expected to include most of the currently existing MP structures while still allowing variability at non-conserved sequence positions, we studied the representative protein clusters compiled in the UniRef50 database. First, we provide an overview of MP size distribution for eukarya and bacteria. For bacteria, the distribution peaks at  $n = 6$ , which is earlier than for eukarya for which a large number of MP entries was obtained until  $n = 7$  (Fig 1A). When excluding MP with  $n = 1$ , 73.8% of sequences fall within  $2 \leq n \leq 6$  in bacteria, whereas 75.0% of eukaryotic sequences reside within  $2 \leq n \leq 7$  and only 61.0% within  $2 \leq n \leq 6$ . Eukarya further employ a higher percentage of large MP ( $n \geq 8$ ) than bacteria. MP numbers decrease substantially for  $n > 12$  with eukarya again exhibiting larger counts than bacteria. Thus, eukarya may operate with more complex MP than bacteria.

Bacteria have larger absolute number of sequences in the UniRef50 database (Fig 1A), however, this is likely a reflection of a wider coverage of sequence space rather than a larger number of unique MP folds. Moreover, a wider coverage does not mean that AA diversity is higher in bacteria than eukarya. AA diversity, evaluated by the Shannon equitability index ( $E_H$ ) is in fact lower in bacteria than in eukarya for all  $n$  (Fig 1B), further suggesting that eukaryotic MP are chemically more complex than their prokaryotic relatives. The wide bacterial coverage of sequence space with a smaller set of preferred AA can arise from extensive AA permutations at non-conserved sites.

### Preferences in AA position along the membrane normal indicate recurring MP architectures and the ability of AA to partake in helix-helix interactions

Before examining AA frequencies, termed  $f$ , as a function of  $n$ , we investigated select  $f(n)$  profiles that were expanded to individual residue positions along the membrane normal, termed

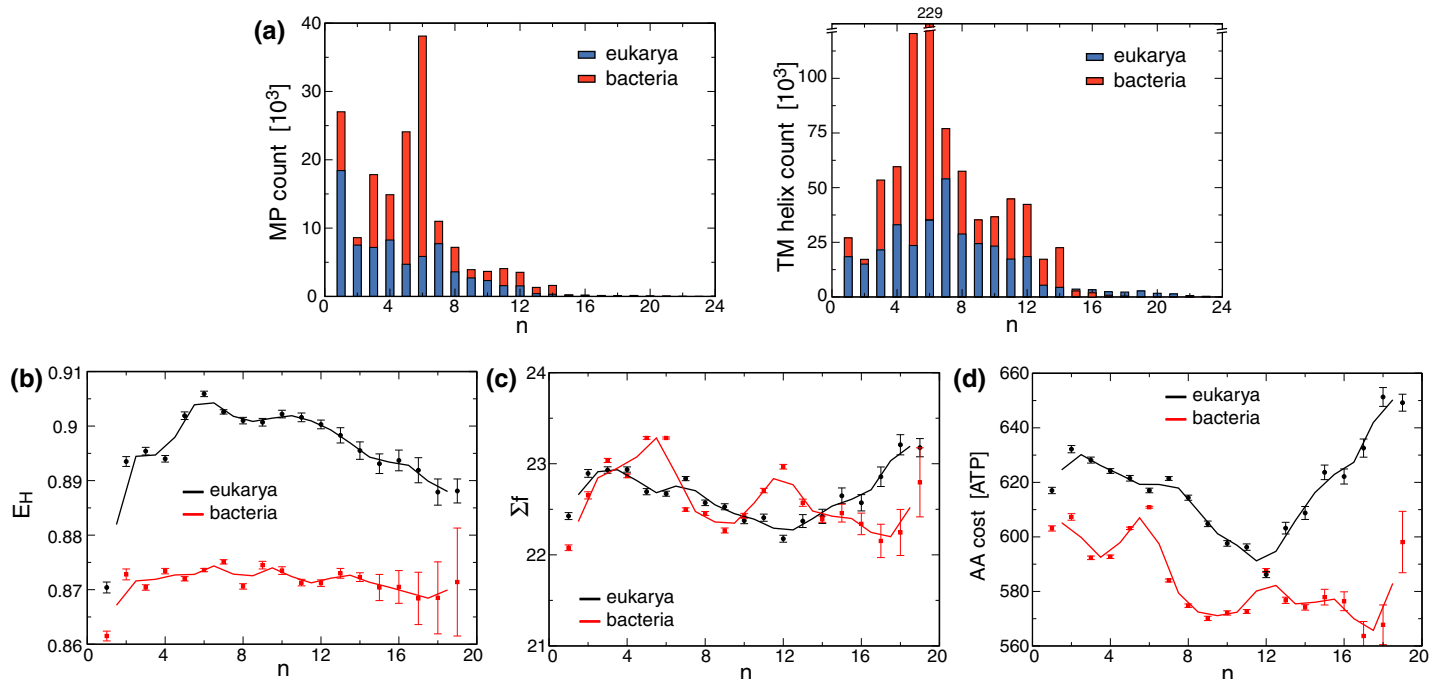


**Fig 1. Select membrane protein parameter as a function of  $n$  in eukarya and bacteria.** (a) Size distribution of MP. The protein count and the count of the total number of TM helices are depicted as a function of  $n$  for  $n \leq 23$ . (b-d) AA diversity quantified by the Shannon equitability index ( $E_H$ ), TM helix length ( $\Sigma f$ , i.e., sum of  $f$  over all AA), and AA cost per TM helix in terms of high-energy phosphate bonds (ATP) are shown as a function of  $n$  for  $n \leq 19$ . Solid lines depict running averages calculated with a window size of two. The  $n$  range was limited because of the scarcity of MP for very large  $n$ .

<https://doi.org/10.1371/journal.pone.0221372.g001>

$m$ , with the TM helix center taken as  $m = 0$ . Studies of immersion depth preferences of AA provide valuable insight into MP architecture [15–18]. The  $f(1,m)$  profile of Gly for example discerns the common GxxxG helix-helix association motif [13] within the N-terminal half of TM helices of eukarya ( $m = -1, -5$ ; S1A Fig). In Asn of eukarya,  $f(n,m)$  profiles exhibit distinct peaks for  $f(2,-1)$  and  $f(7,4)$  whereas for Pro in bacteria  $m = -7, 0$  and  $m = -4, 0$  stand out for  $n = 2$  and  $n = 7$ , respectively (Fig 2A and 2B). As another example, Tyr of eukarya shows a conspicuous peak at  $f(7,-4)$  (Fig 2D). The recurring use of certain  $m$  positions in helix-helix interactions and their specific variation with  $n$  may be useful for understanding and modeling the underlying MP architectures.

The  $f(n,m)$  profiles of a number of residues identified pronounced  $f$  differences between peripheral and center positions. For example, the highest  $f$  values of Asn were found near the membrane border irrespective of  $n$  in confirmation of an important role in TM helix capping (Fig 2A). In addition, the well-established preference of Trp and Tyr for lipid headgroups [19–21] was reflected by high and low frequencies for peripheral and center  $m$ , respectively, and contrast the even  $f(m)$  profile of Phe (Fig 2C–2E). Nonetheless, with increasing  $n$ , Trp and Tyr behaved differently. For Trp, peripheral  $f$  dropped significantly and central  $f$  rose modestly. In contrast, Tyr maintained high peripheral  $f$  and substantially increased central  $f$ . For assembled MP, helix-lipids contacts decrease with increasing  $n$  (for example, see Fig 3A, 3C and 3D). Any anchors that merely stabilized individual helices in the course of folding must, upon assembly, invariably partake in helix-helix interactions. Accordingly, we ascribe the enduring usefulness of Tyr at high  $n$  to an ability to partake in helix-helix interactions, whereas Trp appears less capable in this respect. Although Trp is a stronger anchor than Tyr [20, 21], a more facile integration of Tyr into helix bundles may contribute to its more frequent use than Trp.

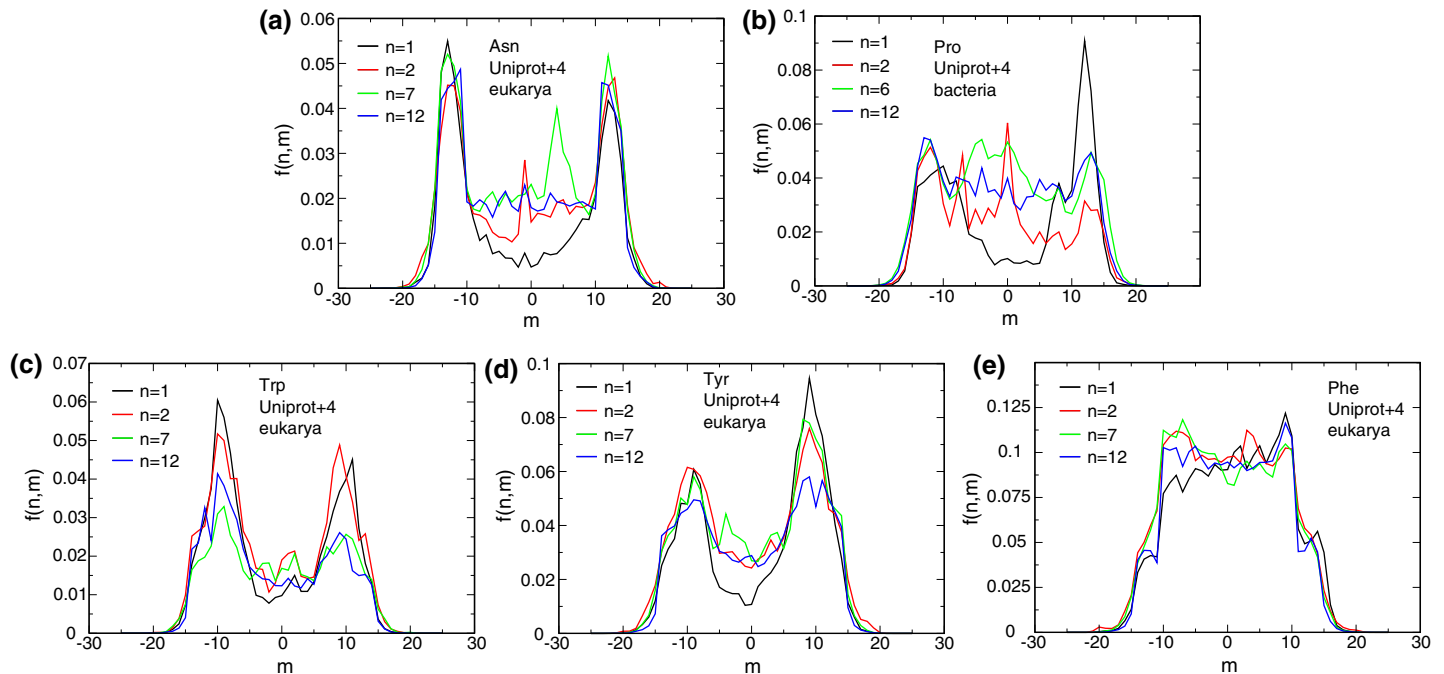


**Fig 2. Amino acid frequencies relative to the center of the membrane.**  $f(n,m)$  profiles of Asn, Trp, Tyr and Phe for eukarya and Pro for bacteria for  $n = 1, 2, 7$  and  $12$ .  $m$  denotes the residue number relative to the predicted TM helix center. Negative and positive  $m$  values indicate orientations toward the N- and C-terminus, respectively, and do not relate to extra- and intracellular orientations. Fixed UniRef50/Uniprot TM helix borders were used and extended by four residues on either helix side.

<https://doi.org/10.1371/journal.pone.0221372.g002>

### Uncertainties in TM helix predictions still permit the reliable assessment of relative $f(n)$ changes

The TM border predictions contained in the UniRef50/UniProt records employed herein are generally based on sequence-based computational predictions [2, 8]. We have assessed the accuracy of such predictions by comparing them to structure-based predictions (Fig 3A) [22, 23] and evaluated the impact of resulting uncertainties on  $f(n)$ . An uncertainty of sequence-based TM border predictions of 3.8 residues was estimated (see Methods) and Monte Carlo simulations were performed to assess the impact of this uncertainty on  $f(n)$ . For residues that tend to be more abundant outside than inside of the membrane,  $f$  values increased and *vice versa* (Fig 3B and S2 Fig). In case of charged residues, this trend involved changes by up to a factor of two. Nonetheless, even for these extreme changes in absolute  $f$  values, relative  $f(n)$  changes were little affected for  $n \geq 2$ . As an alternative assessment, TM helices were uniformly shrunk by four residues from UniRef50/UniProt borders in order to exclude most residues outside of the membrane. With lesser residues in the TM helices, absolute  $f$  values decreased for all residues (Fig 3B and S2 Fig). However, consistent with mere offsets, changes in relative  $f(n)$  were again small. The largest change in relative  $f(n)$  was seen for Trp, which is explained by the overrepresentation of this residue in the lipid headgroup region (Fig 2C). Thus,  $f(n)$  trends can be reliably computed and the Monte Carlo dataset, which includes the lipid headgroup region, was chosen for further analysis.

Next to  $f$  uncertainties from TM borders, such uncertainties can also arise from ambiguities in  $n$  predictions. Marginally hydrophobic helices may evade computational detection, unduly lowering  $n$ . Similarly, any MP oligomerization is not taken into account and would effectively increase  $n$ . Finally, the complexity of MP structures themselves can give rise to  $n$  uncertainties

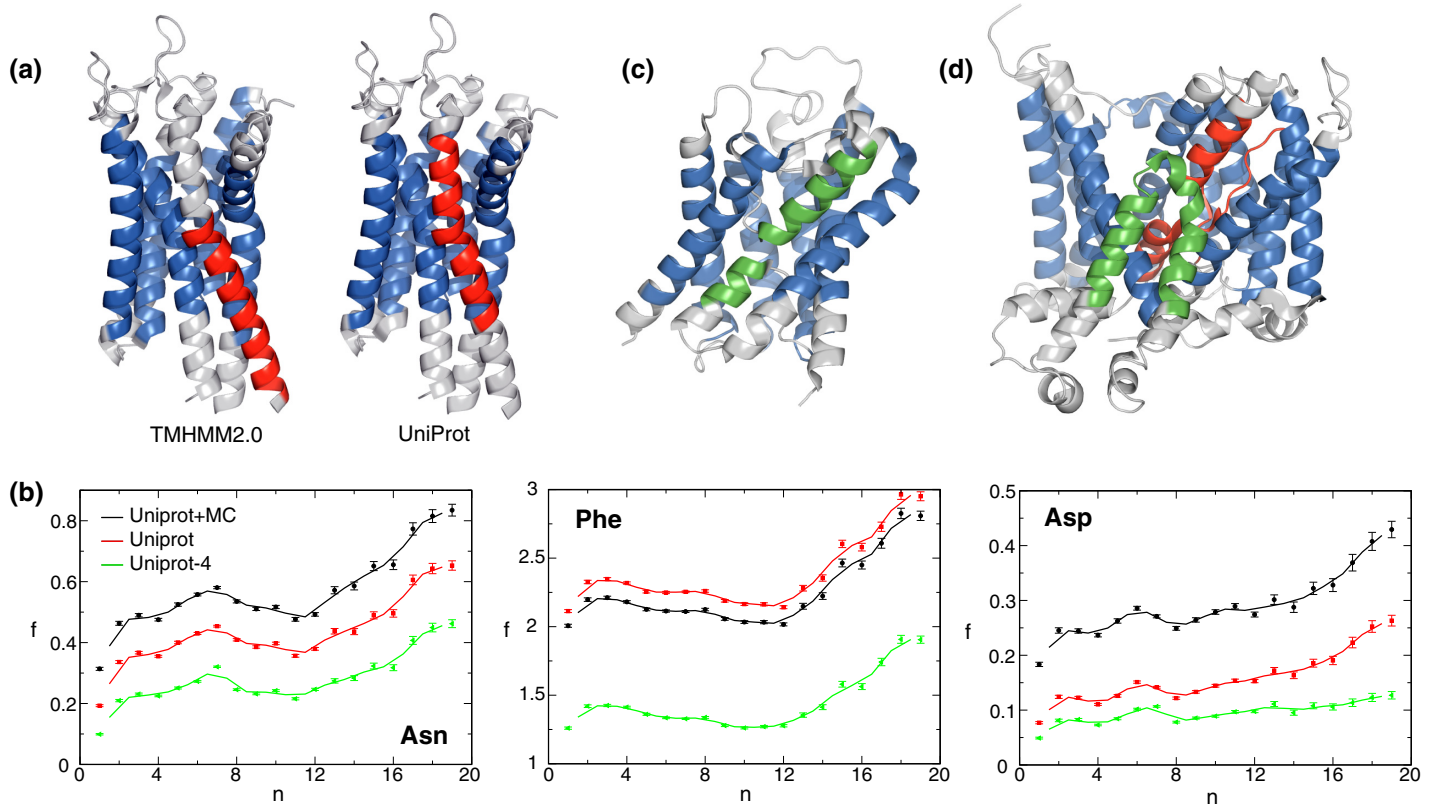


**Fig 3. Illustration of uncertainties and ambiguities in transmembrane helix definitions.** (a) Comparison of TM helix predictions between UniRef50/UniProt and TMHMM 2.0 for the human free fatty acid receptor 1 (FFAR1; PDB entry 4phu). Helix 5 is shown in red and the other TM helices in blue. UniProt and TMHMM predictions of helix 5 encompass residues 179–200 and 188–210, respectively. (b) For the depicted AA,  $f(n)$  was calculated using UniProt TM borders plus Monte Carlo simulations (black), UniProt TM borders (red), and UniProt TM borders shrunk by four residues on each side (green), respectively. Solid lines show running averages calculated with a window size of two. The  $n$  range was limited to  $\leq 19$  because of the scarcity of MP for large  $n$  (Fig 1A). (c) Structure of Aquaporin from *Methanothermobacter marburgensis* (AqpM; PDB entry 2f2b). The intramembranous helices are colored in green and TM helices in blue. AqpM is annotated as  $n = 6$  but its structure reveals that two short intramembrane helices combine to form the functional equivalent of a seventh TM helix. (d) Structure of the C-terminal membrane domain of the human erythrocyte anion exchanger 1 (Band 3; PDB entry 4yzt). The intramembranous helices are colored in green, discontinuous TM helices in red and regular TM helices in blue. In addition to its 12 TM helices and UniRef50/UniProt  $n = 12$  annotation, Band 3 contains two relatively long intramembraneous helices and has been considered to have the equivalent of 14 TM helices [24]. Moreover, Band 3 exhibits two unusual, discontinuous TM helices, where helical conformation breaks down near the center of the membrane, which is then traversed in extended conformations.

<https://doi.org/10.1371/journal.pone.0221372.g003>

(Fig 3C and 3D). Uncertainties in  $n$  misclassify the contribution of affected MP to  $f(n)$ , which would make transitions between adjacent  $f(n)$  values less distinct. However, clear  $f(n)$  trends are discernible at the current level of  $n$  accuracy (Fig 4).

### **$f(n)$ trends in eukarya reveal functional AA groupings and identify three n regions of distinct MP assembly principles**

For Leu, Met, Ile, Val and Phe,  $f(n)$  decreases almost linearly or remains flat up up to  $n = 12$  after which this trend breaks down and a substantial increase in hydrophobic residues is observed (Fig 4A and 4B). Apparently, the previously prevailing MP assembly principles changed to accomplish the folding of very large MP. In the  $1 \leq n \leq 12$  range,  $f_{\text{hydrophobic}} = f_{\text{Leu}} + f_{\text{Met}} + f_{\text{Ile}} + f_{\text{Val}} + f_{\text{Phe}}$  decreased by 13.2% (Fig 5A), which does not correspond to the large reduction in lipid-exposed surface area in the folded state of MP (Fig 3C and 3D). A lower  $f_{\text{hydrophobic}}$  limit may arise from the requirement to embed most individual TM helices in the membrane in the unfolded MP state [25]. Complementary to the decrease of  $f_{\text{hydrophobic}}$ , the frequency of polar residues increased with  $n$  albeit only initially.  $f$  values of Cys, His, Thr, Ser and Asn

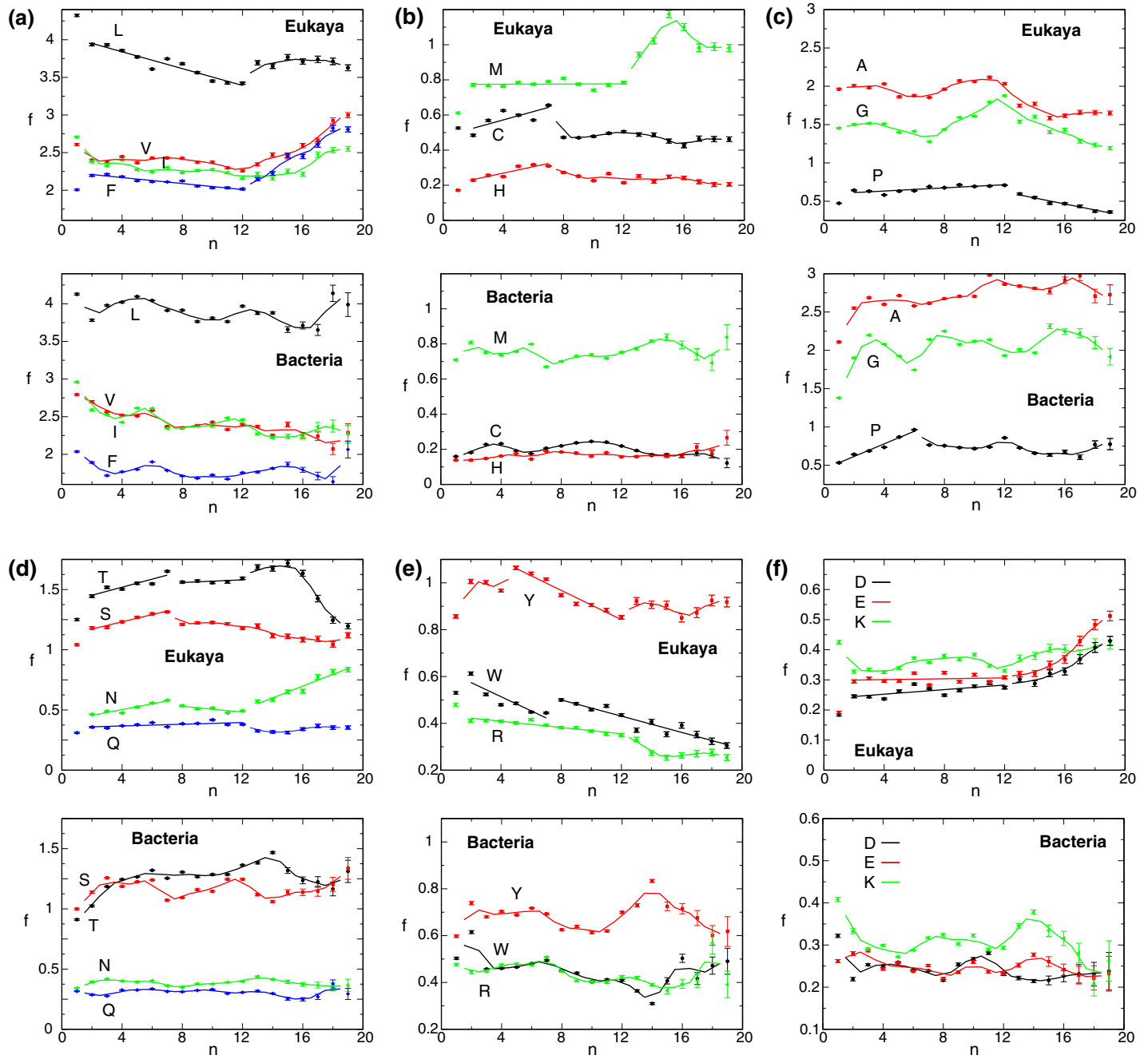


**Fig 4. Transmembrane amino acid frequencies as a function of  $n$  for eukarya and bacteria.** To illustrate  $f(n)$  trends, solid lines depict either linear fits or running averages calculated with a window size of two. The  $n$  range was limited to  $\leq 19$  because of the scarcity of MP for large  $n$  (Fig 1A). Additional taxon-specific plots are provided in S3–S7 Figs.

<https://doi.org/10.1371/journal.pone.0221372.g004>

increased linearly up to  $n = 7$  and, thereafter, mainly decreased (Fig 4B and 4C). Only Gln showed a consistent but less steep  $f$  increase up to  $n = 12$ . For  $n \geq 13$ ,  $f$  trends often changed again and initial  $f$  values were even superseded for Thr and Asn. Next to the  $f_{\text{hydrophobic}}$  division between  $2 \leq n \leq 12$  and  $n \geq 13$ , the breaks in  $f_{\text{polar}}$  trends identify further differences in prevalent MP stabilization between  $2 \leq n \leq 7$  and  $8 \leq n \leq 12$  (Fig 5A).



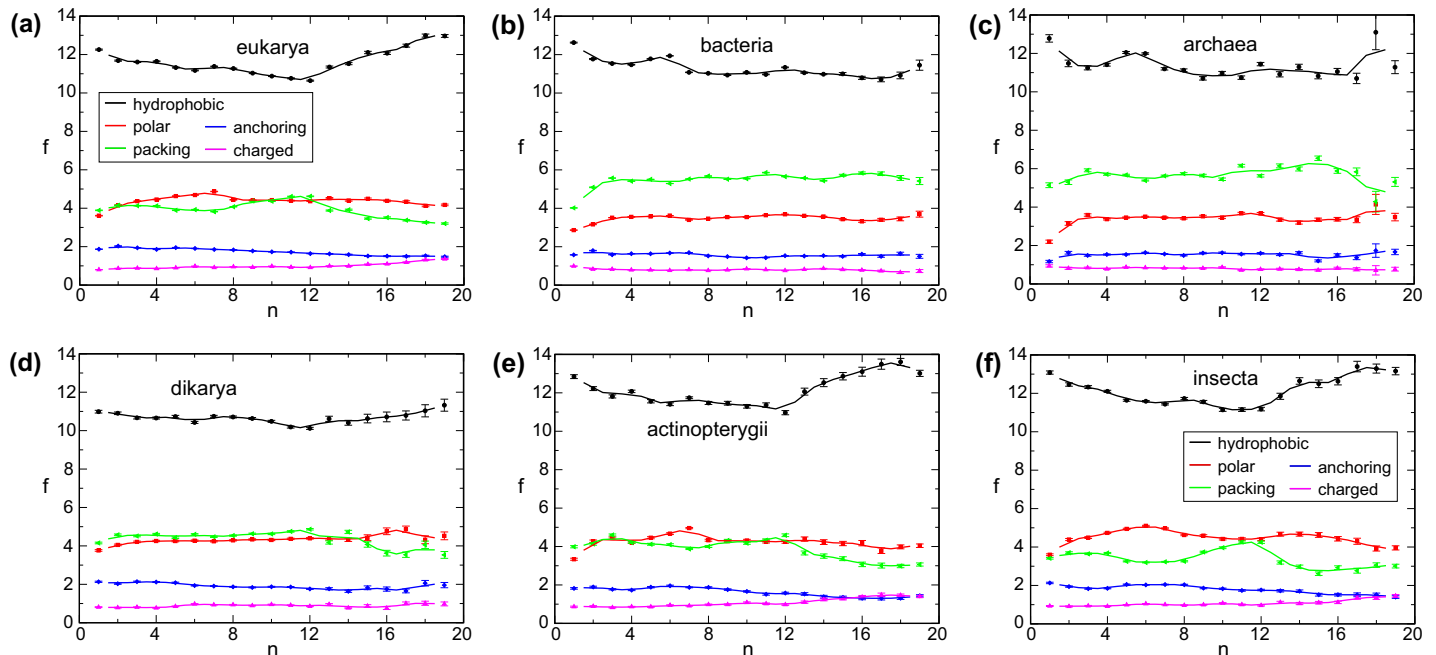


**Fig 5. Transmembrane amino acid frequencies as a function of  $n$  for functional amino acid groupings.**  $f(n)$  of hydrophobic (Leu, Met, Ile, Val and Phe), polar (Cys, His, Asn, Gln, Ser and Thr), packing (Ala, Gly and Pro), anchoring (Trp, Tyr and Arg), and charged (Asp, Glu and Lys) residues were combined for each of the depicted biological taxon. Solid lines show running  $f(n)$  averages calculated with a window size of two. The  $n$  range was limited to  $\leq 19$  because of the scarcity of MP for large  $n$  (Fig 1A).

<https://doi.org/10.1371/journal.pone.0221372.g005>

Gly and Pro have prominent roles in the packing of TM helices [9–11, 13, 14]. As such,  $f_{\text{Gly}}$  and  $f_{\text{Pro}}$  may increase with  $n$ . Except for a slight weakness at  $n = 3$ , this expectation was fulfilled by Pro up to  $n = 12$  (Fig 4C). For Gly, an initial  $f$  uptrend reversed at  $n = 3$  to reach a local minimum at  $n = 7$  but substantially increased again up to  $n = 12$ . It appears that Gly, as  $f_{\text{polar}}$  increased for  $2 \leq n \leq 7$ , was not in high demand but became more useful as  $f_{\text{polar}}$  diminished for  $8 \leq n \leq 12$ . For  $n \geq 13$ , both  $f_{\text{Gly}}$  and  $f_{\text{Pro}}$  trends changed and became less frequent. Above, we did not classify Ala as a hydrophobic residue [26]. Because of its small methyl side chain, Ala may constitute a passive, hydrophobic or a packing-mediating, structural residue like Gly. The  $f(n)$  pattern of Ala followed Gly and not hydrophobic residues (Fig 4A and 4C), suggesting that it still can encode helix-helix packing interactions. Nonetheless, its shallower  $f(n)$  pattern compared to Gly is noted, which indicates less favorable packing interactions compared to Gly. We thus identify Ala as a packing residue and reveal a complementary and largely balanced nature of  $f_{\text{packing}}$  and  $f_{\text{polar}}$  in eukaryotic MP (Fig 5A and 5D–5F).

Similar to the lower limit of  $f_{\text{hydrophobic}}$ , any decrease of  $f_{\text{Trp}}$  and  $f_{\text{Tyr}}$  may be limited by a need to anchor TM helices in the unfolded MP state. For Trp, this expectation was not fulfilled;  $f_{\text{Trp}}$  decreases significantly for  $2 \leq n \leq 7$  due to mostly lower frequencies in headgroup regions (Fig 2C), and this trend continues for  $n \geq 8$  but less steeply. In contrast,  $f_{\text{Tyr}}$  remains near maximal values even in headgroup regions up to  $n = 7$  (Figs 2D and 4E). Nonetheless, beginning at  $n = 5$   $f_{\text{Tyr}}$  also decreases approximately linearly up to  $n = 12$ , after which  $f_{\text{Tyr}}$  recovers somewhat and remains nearly constant. The divergent  $f_{\text{Trp}}$  and  $f_{\text{Tyr}}$  behaviors reinforce our view that Tyr is easier to integrate into TM helix bundles than Trp.

Charged residues also populate lipid headgroup regions where anionic residues contribute to MP anchoring [27, 28]. Asp, Glu and Lys exhibit similar  $f(n)$  behaviors; a tendency for a slow  $f$  increase in the  $2 \leq n \leq 12$  region that becomes more pronounced for  $n \geq 13$  (Fig 4F). In

contrast, Arg shows a decreasing  $f$  trend that becomes pronounced for  $n \geq 13$  (Fig 4E). This trend is more similar to the amphiphilic Trp and Tyr anchors than charged Asp, Glu, and Lys. In accordance with the delocalized charge of its guanidino group, Arg may have higher amphiphilic capabilities than these residues, which may be useful in the context of some lipid interactions [29, 30]. We further note that Arg has the highest  $f$  values among charged residues for small  $n$ . Based on the similarity of Arg with Trp and Tyr, we included it in  $f_{\text{packing}}$  and employed  $f_{\text{charged}}$  solely for Asp, Glu and Lys.

In sum, the  $f(n)$  profiles of eukaryotic MP suggest a functional AA grouping into hydrophobic (Leu, Met, Ile, Val and Phe), polar (Cys, His, Asn, Gln, Ser and Thr), packing (Ala, Gly and Pro), anchoring (Trp, Tyr and Arg), and charged (Asp, Glu and Lys) residues. The corresponding  $f(n)$  trends indicate the existence of three  $n$  regions with distinct MP assembly principles:  $2 \leq n \leq 7$ ,  $8 \leq n \leq 12$  and  $n \geq 13$ .

### Bacterial MP rely on packing over polar interactions

In bacteria, the clearest indication of an increasingly integrated TM helix bundles is provided by  $f_{\text{Pro}}$  for  $1 \leq n \leq 6$  (Fig 4C). This frequency rose from approximately 0.5 to 1 before dropping and staying near 0.75. For  $n = 1$ , it experienced large contributions originating in lipid headgroups (Fig 2B) indicative of helix capping and linker modulation [31]. For higher  $n$ , central positions became abundant, confirming Pro to aid the tight packing of TM helix bundles [10, 11]. Like in eukarya,  $f_{\text{Gly}}$  and  $f_{\text{Ala}}$  appears cyclical and, after an initial rise, forms a local minimum for  $n = 6$ . In accordance with the drop in bacterial MP structures after  $n = 6$  (Fig 1A), it appears that the prevailing MP assembly principles already changed at this earlier  $n$  value. A second distinction from eukaryotic MP is the slow rise of  $f_{\text{polar}}$  (Fig 5A and 5B). For example, for Asn, Ser, and Cys,  $f$  rises only up to  $n = 3$  and remains relatively steady thereafter (Fig 4B and 4D). For Ser, Thr, Trp, and Tyr there is again a change in  $f$  trends at  $n = 12$ , which warrants a distinction of MP architecture between  $7 \leq n \leq 12$  and  $n \geq 13$ , although this transition is less pronounced than for eukaryotic MP. Further differences to eukarya were present in anchoring profiles;  $f_{\text{Trp}}$ ,  $f_{\text{Tyr}}$  and  $f_{\text{Arg}}$  increased up to  $n = 7$  before declining and increasing again for large  $n$  (Fig 4E). Moreover,  $f_{\text{charged}}$  gravitated to lower values with increasing  $n$  in contrast to the eukaryotic trend (Fig 4F). Next to differences in relative  $f$  trends, absolute  $f$  values also differed between eu- and prokarya. The absolute  $f_{\text{polar}}$  and  $f_{\text{anchoring}}$  values of bacteria remained below the eukaryotic values in apparent correspondence to the bacterial reliance on  $f_{\text{packing}}$  (Fig 5A and 5B). Thus, there are clear differences in relative  $f$  trajectories between eu- and prokaryotic MP that relate to different size maxima ( $n = 6$  vs  $7$ ) and place different weights on polar and packing interactions in assembling TM bundles.

### Domain formation and definition in MP

For water-soluble proteins, the concept of protein domains acting as independently folded units has been highly successful [32, 33]. In the context of MP, the term domain is often used to describe a subset of TM helices based on a perceived functional context or evolutionary lineage, whereas its folding independence has usually not been verified. For example, the structure-function relationship of the C-terminal membrane domain of the human erythrocyte anion exchanger 1 (Band3) suggests a core and a gate domain (Fig 6A) [24]. However, it is unclear if both domains, which share an extensive interface, would fold independently of each other. Outside of the native cellular and membrane environment of Band3, an inability to fold would be difficult to interpret. Moreover, Band3 fragments encompassing helices 1–8 and 9–14, which could not fold independently because of voids from missing TM helices (Fig 6B), reconstituted enzymatic activity nonetheless [34]. In MP, it may frequently be ambiguous to



differentiate between protein splits and domains. The already folded nature of unassembled, individual TM helices in the membrane may be a source of this ambiguity (and makes individual helices domains, too). Here, we posit that  $f(n)$  trends relate more directly to the ability of MP to form *bona fide* domains.

To create structural diversity in MP, helix-helix crossings and contacts must vary to form helices that are not parallel relative to each other but still packed without voids [35].  $f_{\text{Pro}}$  may be most indicative of the level of such diversity as proline-induced helix kinks are central to tightly pack TM helices [10, 11]. For bacterial MP,  $f_{\text{Pro}}$  increases for  $2 \leq n \leq 6$  before a break to lower  $f_{\text{Pro}}$  occurs (Fig 4C). Similarly, at  $n = 6$   $f$  trends of Ser and Thr break and level off, respectively (Fig 4D). In addition, the  $f_{\text{Gly}}$  trend changes most conspicuously at  $n = 6$  (Fig 4C). Thus, helix bundles with  $n \geq 7$  appear less integrated than  $2 \leq n \leq 6$  proteins, which suggests the formation of a single domain in the latter and raises the possibility of more than one domain in the former range. With smaller absolute  $f_{\text{packing}}$  values than prokaryotic MP, eukarya appear to place more weight on increasing  $f_{\text{polar}}$  values to create structural diversity (Fig 5A and 5B). The polar trend conspicuously broke at  $n = 7$  and mainly diminished (Fig 4), suggesting that helix bundles behaved as an integrated unit in the  $2 \leq n \leq 7$  range. For  $8 \leq n \leq 12$ , the diminishing  $f_{\text{polar}}$  was increasingly compensated by  $f_{\text{packing}}$  in the background of a continued decline of  $f_{\text{hydrophobic}}$  (Fig 5A and 5F). As such, the TM bundle may or may not be organized as a single unit in this  $n$  range. However, the continued decline of  $f_{\text{hydrophobic}}$  suggests that any domain-domain interface is not lipid exposed and, thus, difficult to dissociate. Band3 could fall in this category (Fig 6A). Moreover we make a contextual reference to the difficulty of separating apparent domains in voltage-gated channels [36, 37]. The  $f_{\text{hydrophobic}}$  trend breaks down at  $n = 12$  and increases thereafter to even supersede the values for small  $n$ . Likewise,  $f_{\text{packing}}$  breaks down at  $n = 12$  and Asn, Thr, and Tyr increase again. This could be reconciled by two or more domains that do not share a deeply integrated interface. When overlaying the  $n$  ranges of possible domain formation on MP counts (Fig 1A), it appears that only relatively few MP form multiple domains. In conclusion, rather than ascertaining the folding independence criterion, the term domain in MP is perhaps best based on functional, structural, and evolutionary relationships.

### AA diversity, the number of TM helices and TM helix length drive MP diversity

Not only MP counts seem to correlate with the breaks in  $f$  trends but also additional parameter. TM helix lengths, i.e.,  $\Sigma f$ , exhibited local  $n = 5-6$  and 12 maxima for bacteria (Fig 1C). In contrast to eukarya, bacteria may be unable to increase AA diversity, i.e.,  $E_H$ , with  $n$  (Fig 1B) and are left to heighten MP diversity by increasing TM length (Fig 1C). A low AA diversity in bacteria allows for a low metabolic cost of synthesizing the component AA of TM helices (Fig 1D). Nonetheless, the energy investment into lengthening TM helices at  $n = 5-6$  and 12 is apparent. Eukaryotic MP displayed a trend towards shorter TM helices in the  $4 \geq n \geq 12$  range that is reversed for  $n \geq 13$  (Fig 1D). Evidently, eukarya achieve higher  $E_H$  levels than bacteria by using more expensive AA that seemed to eliminate the need for longer TM helices for  $n \leq 12$  (Fig 1D). For both eukarya and bacteria, we note that TM helix costs decrease significantly after MP counts drop off after  $n = 7$  and 6, respectively (Fig 1D). At  $n = 12$ , biosynthetic costs between eukaryotic and prokaryotic MP even matched. Eukaryotic MP also increase  $E_H$  up to  $n = 6$  after which a slow decrease was observed (Fig 1B). Thus, MP complexity is a function of  $n$ ,  $E_H$  and  $\Sigma f$ . Moreover, we interpret the high AA cost and high  $\Sigma f$  in bacteria for  $1 \leq n \leq 6$  as well as the even higher AA costs and high  $E_H$  in eukarya for  $1 \leq n \leq 7$  as efforts to maximize MP diversity in these single-domain  $n$  brackets. In contrast for larger MP, AA cost,  $\Sigma f$ , and  $E_H$  mostly decline up to  $n = 12$  (Fig 1B and 1D) further indicating that the increase of  $n$  is

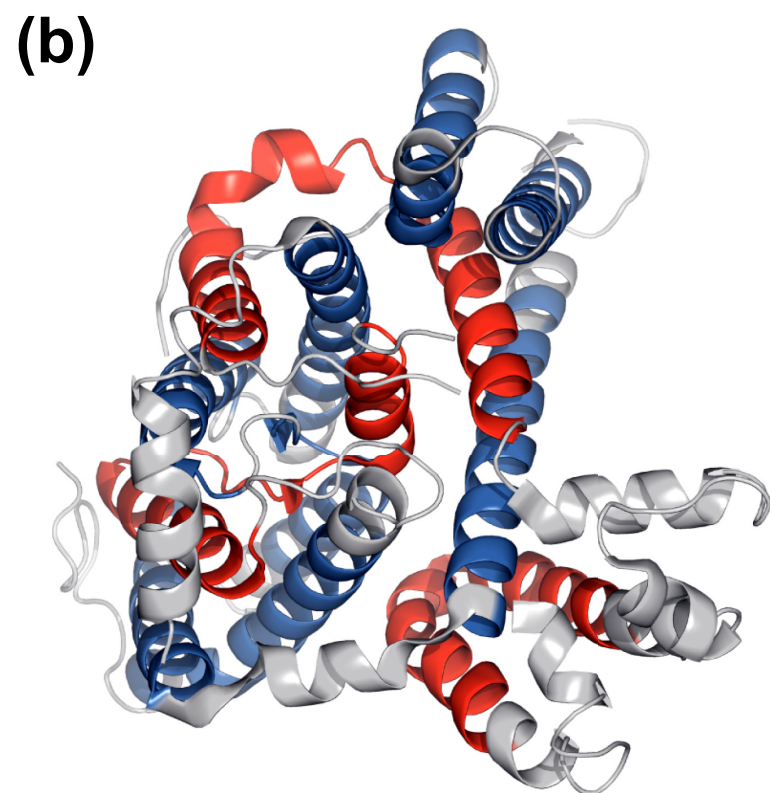
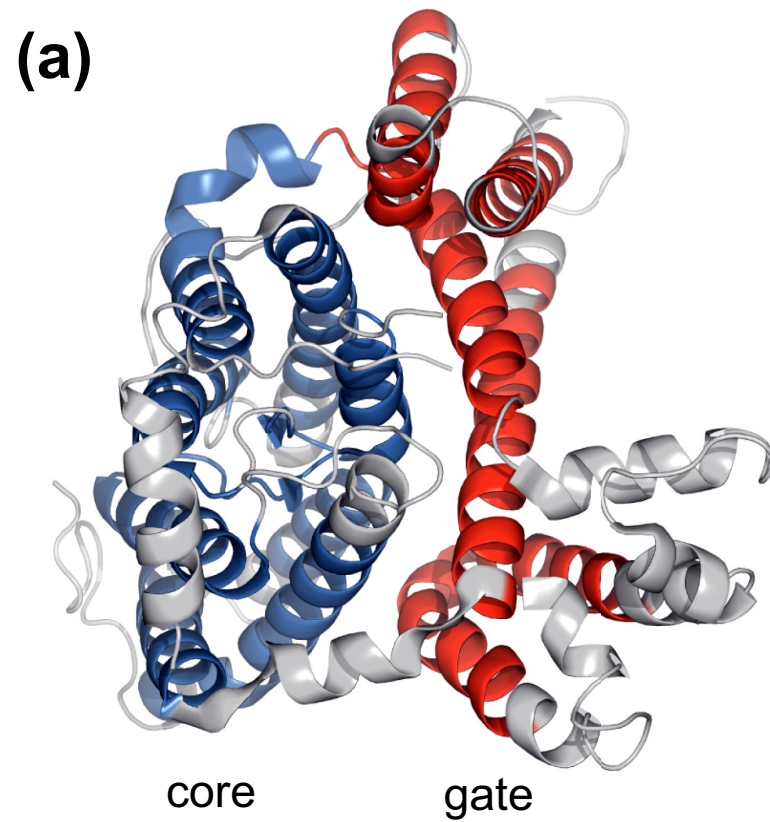


**Fig 6. Domain definition in the C-terminal membrane domain of the human erythrocyte anion exchanger 1 (Band3).** Band 3 carries out chloride/bicarbonate anion exchange across the plasma membrane of erythrocytes [24]. (a) A core (helices 1, 2, 3, 4, 8, 9, 10, and 11) and a gate (helices 5, 6, 7, 12, 13, and 14) domain were differentiated in Band3 [24]. (b) Nonetheless, enzymatic activity of Band3 can be reconstituted by fragments encompassing helices 1–8 and 9–14, shown in blue and red, respectively [34].

<https://doi.org/10.1371/journal.pone.0221372.g006>

sufficient to achieve MP diversity. At  $n = 12$  bacteria form an exception to this statement by adopting unexpectedly high  $\Sigma f$  in apparent requirement of heightened diversity. In eukarya, even larger MP ( $n \geq 13$ ) finally rely on high  $\Sigma f$  instead of high  $E_H$  at nonetheless relatively high overall AA costs.

### AA frequencies in MP are taxa specific and adopt universal ratios

The apparent reliance of bacteria on packing interactions in combination with a scarcity of polar contacts is shared by archaea (Fig 5B and 5C). This may mean that prokaryotes cannot incorporate marginally hydrophobic helices to the same extent as eukarya and that even a modest increase of polar interactions can avoid the need for extensive packing interactions. Moreover, the later peak of eukaryotic as compared to bacterial MP sizes ( $n = 7$  vs 6; Fig 1A) may signal that, by balancing  $f_{\text{packing}}$  and  $f_{\text{polar}}$ , larger and more complex MP can be formed within a single domain. Notwithstanding these statements, we also found  $f_{\text{packing}}-f_{\text{polar}}$  differences between eukaryotic taxa (Fig 5D and 5E). In fact, we found that the frequencies of most AA were correlated and taxa-specific. A specific  $f_{\text{Phe}}$  for instance not only restricts the possible taxa associated with an MP but also puts tight limits on the frequencies of most other residues. For example,  $f_{\text{Ala}}-f_{\text{Phe}}$  are anti-correlated and fit a linear relationship (Fig 7A). It thus appears that the large  $f$  discrepancies between bacteria and eukarya are the result of a gradual evolutionary process.

To describe the correlation between AA frequencies systematically, we have ordered AA along the magnitudes of their correlation coefficient, termed  $R$ , from linear fits with a reference AA in the  $2 \leq n \leq 7$  range. We chose Phe because it gave the largest sum of  $R^2$  of all AA. The comparison of  $R$  shows that, with increasing  $f_{\text{Phe}}$ , the frequencies of Ala, Gly, Pro, Arg, Val and Leu decrease, Trp is little changed, whereas Asp, Thr, Ile, Met, Gln, Ser, His, Cys, Lys, Glu, Asn and Tyr increase (Fig 7B). This pattern bears some resemblances to the order in which AA were presumably added to the genetic code [38–40]. It is assumed that AA that have been absent from the prebiotic environment were added later, once enzymes for their biosynthesis evolved [41]. Phe is a "new" AA and its rise led to the decrease of "old" AA. In the

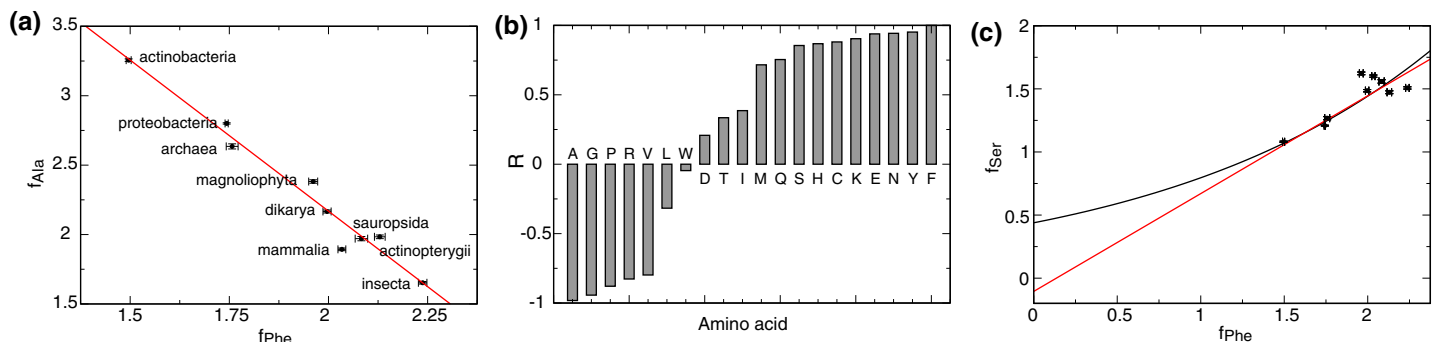


**Fig 7. Taxa-specific correlations between pairwise amino acid frequencies (universal ratios).** The frequencies of most AA are correlated with each other and with taxonomic association. (a) In the  $2 \leq n \leq 7$  range,  $f_{\text{Phe}}$  and  $f_{\text{Ala}}$  of the nine taxonomic groups shown were averaged and correlated using linear equations (S1 Table). (b) The magnitudes of the correlation coefficient, termed  $R$ , of analogous linear  $f_X-f_{\text{Phe}}$  fits are shown (S8 Fig). (c) While it is difficult to ascertain  $f_X-f_{\text{Phe}}$  non-linearity for  $f_{\text{Phe}} \geq 1.5$ , differences between linear and exponential fits become pronounced for  $f_{\text{Phe}} < 1.5$  as illustrated (see also S8 and S9 Figs and S1 and S2 Tables).

<https://doi.org/10.1371/journal.pone.0221372.g007>

evolution of mostly soluble proteins,  $f_{\text{new}}-f_{\text{old}}$  anti-correlations have been documented and referred to as the universal trend [39, 42, 43]. In analogy, we refer to the detected  $f_X-f_{\text{phe}}$  ratios in MP as universal ratios (S1 and S2 Tables).

### Balancing packing and polar interactions likely benefitted the evolution of complex organisms

With  $f_{\text{packing}}$  made up of the old AA Ala, Gly and Pro and  $f_{\text{polar}}$  comprised of mostly new AA, it is unclear whether  $f_{\text{packing}}-f_{\text{polar}}$  balancing is just a byproduct of nearly net neutral evolution or, in relation to functional advantages, drivers of the observed evolution. The phenotypical complexity of organisms in each of the examined taxa broadly increases with  $f_{\text{polar}}$ ; simple unicellular prokaryotes gave rise to more complex unicellular eukaryotes, which led to plants and metazoa that formed the most complex taxa (Fig 8A). Consequently, the  $f_{\text{polar}}$  coordinate relates to evolutionary history. Previously, AA frequencies were proposed to relate to the number of accepted mutations with the number of speciation events (node number) that led to an organism as indicator of this process [44]. For the node number of model organisms, we observed a correlation with taxa-specific  $f_{\text{polar}}$  except for dikarya and magnoliophyta that adopted higher  $f_{\text{polar}}$  values than expected (Fig 8B). These outliers indicate that a rise of  $f_{\text{polar}}$  at the expense of  $f_{\text{packing}}$  was advantageous; the elevated  $f_{\text{polar}}$  achieved AA diversities for dikarya and magnoliophyta that resemble the other examined eukaryotic taxa (Fig 8C). As discussed above, eukarya can form larger and more complex MP than prokarya within a single domain. In other words, although prokarya use all 20 AA they may not take full advantage of AA diversity. Moreover, when comparing the number of UniRef50 entries for model organisms from

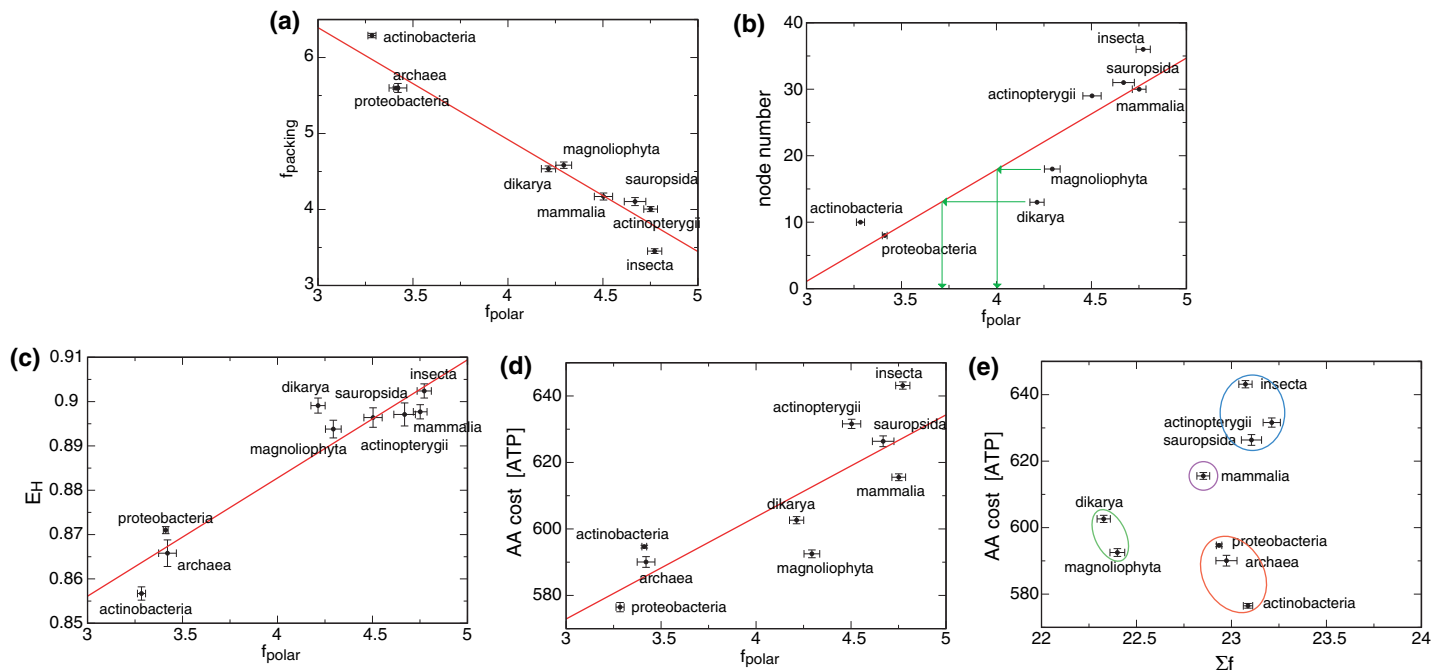


**Fig 8. Correlation of membrane protein and evolutionary parameters with taxa-specific polar AA frequencies.** To gain insight into MP structural parameter, AA composition, and evolution,  $f_{\text{polar}}$  was correlated with  $f_{\text{packing}}$ , node number, AA diversity ( $E_H$ ), and AA cost for the nine taxonomic groups shown. Additionally, AA cost was correlated with TM helix length ( $\Sigma f$ ). If applicable, the examined parameters were averaged in the  $2 \leq n \leq 7$  range. Node numbers of taxa refer to the node numbers (number of speciation events) of corresponding model organisms shown in Table 1 and were taken from ref. [44]. AA cost refers to the AA cost per TM helix in terms of high-energy phosphate bonds (ATP) [45]. AA diversity is quantified by the Shannon equitability index ( $E_H$ ). TM helix length is the sum of  $f$  over all TM AA.

<https://doi.org/10.1371/journal.pone.0221372.g008>

Table 1. Number of examined membrane proteins per taxonomic group.

Taxonomic group	Number of examined membrane proteins (UniRef50 entries) for taxonomic group	Model organism representing taxonomic group	Number of examined membrane proteins (UniRef50 entries) for model organism
Bacteria	167,292	–	–
Eukarya	73,363	–	–
Actinobacteria	24,441	<i>Mycobacterium tuberculosis</i>	310
Proteobacteria	72,224	<i>Escherichia coli</i>	847
Archaea	5,812	<i>Haloferax volcanii</i>	106
Magnoliophyta	8,850	<i>Arabidopsis thaliana</i>	2,602
Dikarya	10,581	<i>Saccharomyces cerevisiae</i>	1,011
Mammalia	13,349	<i>Homo sapiens</i>	4,924
Sauropsida	4,503	<i>Gallus gallus</i>	944
Actinopterygii	6,194	<i>Danio rerio</i>	1,421
Insecta	10,111	<i>Drosophila melanogaster</i>	909

<https://doi.org/10.1371/journal.pone.0221372.t001>

each taxa, eukarya utilize more MP than prokarya although *E. coli* comes close (Table 1). We hypothesize that, by balancing  $f_{\text{packing}}$  and  $f_{\text{polar}}$ , a larger overall number of unique MP can be constructed, which benefits eukarya on a functional level and contributed to the rise of  $f_{\text{polar}}$ .

The biosynthetically more costly new AA invariably increased AA costs in correlation to  $f_{\text{polar}}$  (Fig 8D). Nonetheless, mammalia, dikarya, and, most notably, magnoliophyta achieved high  $E_{\text{H}}$  levels at relatively low costs; the AA cost of magnoliophyta is even at the level of prokaryotes (Fig 8D). This efficiency is achieved by reducing TM helix length as compared to prokaryotes and other eukaryotes (Fig 8E), which further emphasizes  $\Sigma f$  and  $E_{\text{H}}$  as parameters of MP diversity. On the other hand, actinopterygii, sauropsida, and insecta afforded relatively high costs. While magnoliophyta synthesize essentially all AA *de novo*, dikarya, which still have this ability, are already less affected by cost, suggesting that diversified food networks can reduce the effective AA cost. Such networks may have allowed insecta to achieve the highest  $f_{\text{polar}}$  levels. However, because of the complex lifestyles and multicellular nature of metazoa, it remains ambiguous whether this level reflects a most advanced MP assortment or merely evolutionary history as suggested by their  $f_{\text{polar}}$  correlation with node number (Fig 8B). In sum, we propose that AA preferences of taxa relate to evolutionary history, overall proteome diversity (functional sophistication), and lifestyle, which determines effective AA cost.

### AA composition of extinct MP

The decline of Ala, Gly, Pro, Arg, Val, and Leu as a function  $f_{\text{Phe}}$  (Fig 7A and 7B) suggests that those AA were both present when MP protein synthesis first took place and essential to early MP structures. The remaining AA then rose from either low levels because they became more useful to MP over time or from zero as they were incorporated into the genetic code and became available for the first time. For example, the above listed AA lack Ser and Thr that are believed to precede the presence of Arg in the genetic code (Table 2). Ser and Thr may have risen from low levels in relation to functional demands, an altered chemical environment, or advances in inserting MP into the membrane. The early importance of anionic Arg could relate to its ability to anchor proteins to anionic lipids [28, 46] which supports its classification as an anchoring residue (Fig 4E). Subsequently its decline as the principal anchoring residue resulted from competition with Lys and the emergence of the superior Tyr and Trp anchors.

With the  $f_{\text{Phe}}$  coordinate relating to evolutionary history (Fig 7A), it can be followed back in time to predict the AA composition of the earliest forms of life. We had described  $f_{\text{X}}(f_{\text{Phe}})$  using linear functions for  $f_{\text{Phe}} \geq 1.5$  (Fig 7A and 7B and S8 Fig). However, to allow slower rates

**Table 2. Predicted amino acid composition of primordial membrane proteins.**

AA in order of proposed entry into genetic code <sup>a</sup>	f estimate based on $f_{\text{Phe}} = -2.24^{\text{b,c}}$	f estimate based on $f_{\text{Phe}} = 0^{\text{c}}$
Gly	2.8	2.7
Ala	5.5	4.8
Asp	0.16	0.20
Val	4.7	4.0
Pro	0.94	0.94
Ser	0.12	0.44
Glu	0.05	0.13
Thr	0.75	0.97
Leu	4.9	4.6
Arg	1.2	0.85
Asn	0	0.09
Ile	0	1.1
Gln	0	0.15
His	0	0.02
Lys	0	0.05
Cys	0	0.00
Phe	0	0
Tyr	0	0
Met	0	0
Trp	0	0
SUM	21.1	21.0

<sup>a</sup>according to ref. [38]

<sup>b</sup>assuming the presence of only the first ten AA of the genetic code

<sup>c</sup>calculated using S2 Table

<https://doi.org/10.1371/journal.pone.0221372.t002>

of AA incorporation in earlier evolution ( $f_{\text{Phe}} < 1.5$ ), we modeled  $f_X(f_{\text{Phe}})$  for the wider  $f_{\text{Phe}}$  range using exponential functions (Fig 7C and S9 Fig). Table 2 summarizes the predicted AA frequencies for this model at time  $f_{\text{Phe}} = -2.24$  and when assuming that only the first ten AA were present. Packing, polar and hydrophobic frequencies were estimated at 9.2, 9.6 and 0.9, respectively, implying that structural diversity arose almost entirely from the combinatorial possibilities afforded by packing interactions. The primordial TM helix length was predicted at 21.1 residues (Table 2), which is slightly shorter than their contemporaries (Fig 8E). At time  $f_{\text{Phe}} = 0$ , the genetic code putatively expanded to 16 AA and packing, polar and hydrophobic frequencies adapted to 8.5, 9.7 and 1.7, respectively (Table 2). That is, polar contributions increased at the expense of packing interactions. Most of the polar increases were predicted to stem from increased Ser and Thr frequencies, which may indicate an elevated demand on MP structural diversity. Among the newly acquired AA, Ile was most successful and Gln and Asn added novel polar interactions. At 21.0 AA, the TM length would essentially be unchanged. The low level of new AA means that entropic considerations favor their usage, which may make their rise a byproduct of nearly neutral net evolution. Nonetheless, the steep rise of e.g. Ser and Ile further suggests that evolutionary pressure directly connects to functional advantages. In this context, we point out similar f values for Trp across taxa (Fig 7B). Trp is both assumed to enter the genetic code last [38] and the most costly AA to synthesize [45]. Nonetheless, in apparent association to (a) distinct functional advantage(s), Trp incorporation was essentially complete by the time the accessible  $f_{\text{Phe}}$  window was reached ( $f_{\text{Phe}} = 1.5$ ; S8 and S9



Figs). Finally, we note that the decline of packing and rise of polar AA may be "actively" encouraged by CpG hypermutability [47]. In other words, driving organisms to higher AA diversity would be an evolutionary direction that was successful enough to find a biochemical implementation.

## Conclusions

In the absence of all 20 natural AA, biological organisms operated with conceptually simpler and less diverse MP than extant organisms. For most AA, diversification follows predictable relationships between old and new AA (universal ratios) with the position of biological taxa on the  $f_{\text{polar}}$  coordinate relating to their evolutionary history, proteome diversity, and effective AA cost. As indicated by the sustainability of  $f$  trends to higher  $n$  values relative to bacteria (Figs 4 and 5), the  $f_{\text{packing}}-f_{\text{polar}}$  balances attained by eukarya accomplish a seemingly deeper integration of TM helix bundles (higher level of MP complexity). In other words, more decisive helix-helix interactions per helix appear possible in eukaryotic MP. Further relationships of  $E_H$ ,  $\Sigma f$  and AA cost with  $n$  and taxa reiterate that achievable MP diversity (functional sophistication) and AA cost are the drivers of MP proteome evolution. Moreover,  $E_H$  and  $\Sigma f$  investments in small, single-domain MP of eukarya and bacteria, respectively (Fig 1), indicate an advantage in maximizing MP diversity for these groups ( $2 \leq n \leq 7$  in eukarya). If an MP folds unsuccessfully, it has to be degraded or refolded, which increases effective biosynthetic costs and may have conferred an evolutionary advantage to single-domain MP. However, this circumstance also implies that, if a more efficient folding pathway exists at higher  $n$ , transitions to such  $n$  can be advantageous overall. It is remarkable that the seemingly old-fashioned packing interactions were retained most by eukarya for  $8 \leq n \leq 12$  (Fig 5). The diminished integration of MP bundles in this bracket may indicate that folding pathways became more difficult at higher  $n$  and that packing interactions made them "safer". We therefore propose that foldable MP structures become more limited for  $n \geq 8$  with the majority of  $n \geq 13$  MP no longer able to achieve a deeply integrated helix bundle, resulting in the formation of truly independent domains. In sum, the relatively simple analysis of  $f(n)$  trends and taxonomic  $f$  associations provided fundamentally new insight into MP architecture, composition, and evolution.

## Methods

### Choice of sequence database

As genomes of an increasing number of organisms are sequenced, redundancies arise from closely related sequences. To cover sequence space evenly, clustered databases have been developed [48]. For example, the UniProt Reference Clusters (UniRef) database provides coverage of the sequence space at three resolutions. UniRef100 combines identical sequences and sub-fragments from any organism into a single entry (cluster). A cluster representative is then chosen based on available sequence information [49]. UniRef90 is then built by clustering UniRef100 sequences such that each cluster is composed of sequences with at least 90% sequence identity to and 80% overlap with the seed sequence [49]. UniRef50 is analogously constructed by clustering UniRef90 seed sequences that maintain at least 50% sequence identity to and 80% overlap with the longest sequence in the cluster. Sequences identities that exceed 50% generally exhibit homologous protein structures. As such, UniRef50 is expected to virtually capture all currently existing MP structures. Moreover, on a structural level MP are often homologous at lower sequence similarity, implying that redundancies in protein structure will be present. There are even more stringent databases available [50] but this would fix AA types even at non-conserved sites to the cluster representative. For the purpose of discerning  $f(n)$  trends, blurring the difference between conserved and non-conserved sites was not desired,

therefore our study employed the UniRef50 database. We note that UniRef50 generally uses the best-annotated database entry as cluster representative, which in rare instances produced entries outside of a selected taxonomic group. For example, 1.4% of entries in the bacterial dataset are from eukarya and the eukaryotic dataset exhibits bacterial entries at 0.4% (Table 1). For individual taxonomic classes (Table 1), such entries increased somewhat (2–8%) when also counting annotation ambiguities as foreign entries. However, even the removal of all such entries merely shifted the original  $f(n)$  close to reported uncertainties and to retain even coverage of sequence space  $f(n)$  was calculated with all entries present.

### Calculation of AA frequencies (f)

UniRef50 cluster representatives, which exhibited location tags "Multi-pass membrane protein [SL-9909]" or "Single-pass membrane protein [SL-9904]", protein existence codes 1–3, and the desired taxonomic association were initially selected. UniProt classifies protein existence in five categories ([http://www.uniprot.org/help/protein\\_existence](http://www.uniprot.org/help/protein_existence)) where classes 4 and 5 refer to predicted and uncertain proteins, respectively, which were excluded from analysis. Entries were further required to exhibit "helical" or "discontinuously helical" transmembrane annotations, which resulted in the numbers of examined UniRef50 database entries summarized in Table 1. TM helix border predictions were taken directly from UniProt entries. The frequency,  $f$ , of finding an AA, X, in a TM helix is given by the count of X divided by the number of examined helices. The uncertainty in  $f$  arising from sampling a finite database size (count of examined TM helices) was estimated to be  $2 \cdot \sqrt{(\text{count}/4)}$ . The uncertainty in  $f$  from errors in TM border predictions was estimated using Monte Carlo simulations. For this purpose, the standard deviation between sequence-based TMHMM 2.0 TM border predictions and structure-based estimates contained in UniProt records were calculated for the following proteins: Aquaporin AqpM (PDB: 2f2b, UniProt: AQP\_METTM), heart cytochrome c oxidase (PDB: 5xdq, Uniprot: COX1\_BOVIN), free fatty acid receptor 1 (PDB: 4phu, Uniprot: FFAR1\_human), DsbB (PDB: 2zuq, Uniprot: DSBB\_ECOLI) and facilitated glucose transporter member 3 (PDB: 4zw9, Uniprot: GTR3\_HUMAN). Predicted helix borders of all studied UniRef50 records were then varied randomly within a Gaussian distribution of standard deviation 3.8 with the stipulation that the overall helix length cannot shrink by more than five residues. We gratefully acknowledge the use of the GNU Scientific Library, gnuplot and Grace.

### Calculation of AA diversity and biosynthesis cost of TM helix-constituting AA

The Shannon diversity index ( $H$ ) is defined as  $-\sum p_x \ln p_x$  where the sum extends over all 20 AA and  $p_x$  is the probability of finding residue X in a studied TM helix, i.e.,  $p_x = f_x / \sum f$  where  $\sum f$  denotes the sum of  $f$  for all AA. We report the Shannon equitability index,  $E_H = H / \ln 20$ , as measure of TM helix AA diversity. The metabolic cost in terms of high-energy phosphate bonds of synthesizing the constituent AA of a TM helix is  $-\sum f_x \text{ATP}(X)$  where  $\text{ATP}(X)$  denotes the cost of synthesizing AA X *de novo* in *E. coli* [45] and the sum extends over all 20 AA.

### Supporting information

**S1 Fig. Glycine frequencies along the membrane normal.** (a-b)  $f(1,m)$  profiles of Gly for eukarya and bacteria where  $m$  denotes the residue number relative to the predicted TM helix center. Negative and positive  $m$  values indicate orientations toward the N- and C-terminus, respectively, and do not relate to extra- and intracellular orientations. In eukarya, the helix-helix association motif GxxxG [13] was directly observed in contrast to bacteria where  $f(1,m)$  peaked in the C-terminal helix half and was lowest at the TM helix center. Helices with an

even and uneven number of AA are also plotted separately for reference. Fixed UniRef50/UniProt TM helix borders were used.

(EPS)

**S2 Fig. Influence of TM helix border definitions on TM helix amino acid frequencies.** For each AA,  $f(n)$  was calculated using UniProt TM borders plus Monte Carlo simulations (*black*; see [Methods](#)), UniProt TM borders (*red*), and UniProt TM borders shrunk by four residues on each side (*green*), respectively. Solid lines show running averages calculated with a window size of two. The  $n$  range was limited to  $\leq 19$  because of the scarcity of MP for large  $n$  ([Fig 1A](#)).

(EPS)

**S3 Fig. Transmembrane amino acid frequencies as a function of  $n$  for actinobacteria and archaea.** Solid lines depict running  $f(n)$  averages calculated with a window size of two. The  $n$  range was limited to  $\leq 19$  because of the scarcity of MP for large  $n$  ([Fig 1A](#)).

(EPS)

**S4 Fig. Transmembrane amino acid frequencies as a function of  $n$  for proteobacteria and dikarya.**

(EPS)

**S5 Fig. Transmembrane amino acid frequencies as a function of  $n$  for magnoliophyta and sauropsida.**

(EPS)

**S6 Fig. Transmembrane amino acid frequencies as a function of  $n$  for insecta and actinopterygii.**

(EPS)

**S7 Fig. Transmembrane amino acid frequencies as a function of  $n$  for metazoa and mammalia.**

(EPS)

**S8 Fig. Taxa-specific linear correlations between pairwise amino acid frequencies (universal ratios).** For AA X,  $f_{\text{Phe}}$  and  $f_X$  in the  $2 \leq n \leq 7$  range were averaged for the nine taxonomic groups shown and correlated using  $f_X = a \cdot f_{\text{Phe}} + b$ . Fitted parameters are summarized in [S1 Table](#).

(EPS)

**S9 Fig. Taxa-specific exponential correlations between pairwise amino acid frequencies (universal ratios).** For AA X,  $f_{\text{Phe}}$  and  $f_X$  in the  $2 \leq n \leq 7$  range were averaged for the nine taxonomic groups shown and correlated using  $f_X = a \cdot \exp(b \cdot f_{\text{Phe}}) + c$ . For AA with rising  $f_X$   $c = 0$  was assumed. Fitted parameters are summarized in [S2 Table](#).

(EPS)

**S1 Table. Universal ratios with respect to Phe assuming  $f_X = a \cdot f_{\text{Phe}} + b$ .**

(PDF)

**S2 Table. Universal ratios with respect to Phe assuming  $f_X = a \cdot \exp(b \cdot f_{\text{Phe}}) + c$ .**

(PDF)

## Author Contributions

**Conceptualization:** Tobias S. Ulmer.

**Data curation:** Alan J. Situ.

**Formal analysis:** Tobias S. Ulmer.

**Funding acquisition:** Tobias S. Ulmer.

**Supervision:** Tobias S. Ulmer.

**Visualization:** Alan J. Situ.

**Writing – original draft:** Tobias S. Ulmer.

**Writing – review & editing:** Tobias S. Ulmer.

## References

1. Overington JP, Al-Lazikani B, Hopkins AL. Opinion—How many drug targets are there? *Nat Rev Drug Discov.* 2006; 5(12):993–6. WOS:000242478300012. <https://doi.org/10.1038/nrd2199> PMID: 17139284
2. Krogh A, Larsson B, von Heijne G, Sonnhammer ELL. Predicting transmembrane protein topology with a hidden Markov model: Application to complete genomes. *J Mol Biol.* 2001; 305(3):567–80. WOS:000167760800017. <https://doi.org/10.1006/jmbi.2000.4315> PMID: 11152613
3. Wiener MC, White SH. Structure Of A Fluid Dioleoylphosphatidylcholine Bilayer Determined By Joint Refinement Of X-Ray And Neutron-Diffraction Data.3. Complete Structure. *Biophys J.* 1992; 61(2):434–47. ISI:A1992HC77800014. [https://doi.org/10.1016/S0006-3495\(92\)81849-0](https://doi.org/10.1016/S0006-3495(92)81849-0) PMID: 1547331
4. van Meer G. Cellular lipidomics. *EMBO J.* 2005; 24(18):3159–65. WOS:000232551600001. <https://doi.org/10.1038/sj.emboj.7600798> PMID: 16138081
5. Rothman JE, Lenard J. Membrane Asymmetry. *Science.* 1977; 195(4280):743–53. WOS: A1977CV55700006. <https://doi.org/10.1126/science.402030> PMID: 402030
6. Schulz GE. The structure of bacterial outer membrane proteins. *Biochim Biophys Acta-Biomembr.* 2002; 1565(2):308–17. WOS:000179084900013.
7. White SH, von Heijne G. How translocons select transmembrane helices. *Ann Rev Biophys.* 2008; 37:23–42. WOS:000258107500003.
8. Kall L, Krogh A, Sonnhammer ELL. A combined transmembrane topology and signal peptide prediction method. *J Mol Biol.* 2004; 338(5):1027–36. WOS:000221305200014. <https://doi.org/10.1016/j.jmb.2004.03.016> PMID: 15111065
9. Senes A, Engel DE, DeGrado WF. Folding of helical membrane proteins: the role of polar, GxxxG-like and proline motifs. *Curr Opin Struct Biol.* 2004; 14(4):465–79. WOS:000223780100013. <https://doi.org/10.1016/j.sbi.2004.07.007> PMID: 15313242
10. Schmidt T, Situ AJ, Ulmer TS. Structural and thermodynamic basis of proline-induced transmembrane complex stabilization. *Sci Rep.* 2016; 6:29809. WOS:000379922800001. <https://doi.org/10.1038/srep29809> PMID: 27436065
11. Yohannan S, Faham S, Yang D, Whitelegge JP, Bowie JU. The evolution of transmembrane helix kinks and the structural diversity of G protein-coupled receptors. *Proc Natl Acad Sci U S A.* 2004; 101(4):959–63. WOS:000188533600012. <https://doi.org/10.1073/pnas.0306077101> PMID: 14732697
12. del Val C, White SH, Bondar AN. Ser/Thr Motifs in Transmembrane Proteins: Conservation Patterns and Effects on Local Protein Structure and Dynamics. *J Membr Biol.* 2012; 245(11):717–30. WOS:000310473600007. <https://doi.org/10.1007/s00232-012-9452-4> PMID: 22836667
13. Russ WP, Engelman DM. The GxxxG motif: A framework for transmembrane helix-helix association. *J Mol Biol.* 2000; 296(3):911–9. ISI:000085724500015. <https://doi.org/10.1006/jmbi.1999.3489> PMID: 10677291
14. Dawson JP, Weinger JS, Engelman DM. Motifs of serine and threonine can drive association of transmembrane helices. *J Mol Biol.* 2002; 316(3):799–805. ISI:000174216400027. <https://doi.org/10.1006/jmbi.2001.5353> PMID: 11866532
15. Landoltmarticorena C, Williams KA, Deber CM, Reithmeier RAF. Nonrandom Distribution Of Amino-Acids In The Transmembrane Segments Of Human Type-I Single Span Membrane-Proteins. *J Mol Biol.* 1993; 229(3):602–8. ISI:A1993KM69800005. <https://doi.org/10.1006/jmbi.1993.1066> PMID: 8433362
16. Ulmschneider MB, Sansom MSP. Amino acid distributions in integral membrane protein structures. *Biochim Biophys Acta-Biomembr.* 2001; 1512(1):1–14. ISI:000168735500001.

17. Adamian L, Nanda V, DeGrado WF, Liang J. Empirical lipid propensities of amino acid residues in multi-span alpha helical membrane proteins. *Proteins-Structure Function And Bioinformatics*. 2005; 59(3):496–509. WOS:000228779200010.
18. Baeza-Delgado C, Marti-Renom MA, Mingarro I. Structure-based statistical analysis of transmembrane helices. *Eur Biophys J Biophys Lett*. 2013; 42(2–3):199–207. WOS:000315360500009.
19. Garcia JC, Strube M, Leingang K, Keller K, Mueckler MM. Amino-Acid Substitutions At Tryptophan-388 And Tryptophan-412 Of The Hcp2 (Glut1) Glucose Transporter Inhibit Transport Activity And Targeting To The Plasma-Membrane In *Xenopus Oocytes*. *J Biol Chem*. 1992; 267(11):7770–6. WOS:A1992HN48500081. PMID: 1560011
20. Wimley WC, White SH. Experimentally determined hydrophobicity scale for proteins at membrane interfaces. *Nat Struct Biol*. 1996; 3(10):842–8. ISI:A1996VK99300008. PMID: 8836100
21. Situ AJ, Kang SM, Frey BB, An W, Kim C, Ulmer TS. Membrane Anchoring of alpha-Helical Proteins: Role of Tryptophan. *J Phys Chem B*. 2018; 122(3):1185–94. WOS:000423652900019. <https://doi.org/10.1021/acs.jpcc.7b11227> PMID: 29323921
22. Lomize MA, Pogozheva ID, Joo H, Mosberg HI, Lomize AL. OPM database and PPM web server: resources for positioning of proteins in membranes. *Nucleic Acids Res*. 2012; 40(D1):D370–D6. WOS:000298601300054.
23. Stansfeld PJ, Goose JE, Caffrey M, Carpenter EP, Parker JL, Newstead S, et al. MemProtMD: Automated Insertion of Membrane Protein Structures into Explicit Lipid Membranes. *Structure*. 2015; 23(7):1350–61. WOS:000360312200022. <https://doi.org/10.1016/j.str.2015.05.006> PMID: 26073602
24. Reithmeier RAF, Casey JR, Kalli AC, Sansom MSP, Alguel Y, Iwata S. Band 3, the human red cell chloride/bicarbonate anion exchanger (AE1, SLC4A1), in a structural context. *Biochim Biophys Acta-Bio-membr*. 2016; 1858(7):1507–32. WOS:000377233000012.
25. Popot JL, Engelman DM. Membrane-Protein Folding And Oligomerization—The 2-Stage Model. *Biochemistry*. 1990; 29(17):4031–7. WOS:A1990DB30600001. <https://doi.org/10.1021/bi00469a001> PMID: 1694455
26. Nilsson I, Johnson AE, von Heijne G. How hydrophobic is alanine? *J Biol Chem*. 2003; 278(32):29389–93. ISI:000184507000002. <https://doi.org/10.1074/jbc.M212310200> PMID: 12761228
27. Vonheijne G. Control Of Topology And Mode Of Assembly Of A Polytopic Membrane-Protein By Positively Charged Residues. *Nature*. 1989; 341(6241):456–8. WOS:A1989AT97600062. <https://doi.org/10.1038/341456a0> PMID: 2677744
28. Kim C, Schmidt T, Cho EG, Ye F, Ulmer TS, Ginsberg MH. Basic amino-acid side chains regulate transmembrane integrin signalling. *Nature*. 2012; 481(7380):209–12. WOS:000298981200041.
29. Gleason NJ, Vostrikov VV, Greathouse DV, Koeppe RE. Buried lysine, but not arginine, titrates and alters transmembrane helix tilt. *Proc Natl Acad Sci U S A*. 2013; 110(5):1692–5. WOS:000314558100030. <https://doi.org/10.1073/pnas.1215400110> PMID: 23319623
30. Jiang YX, Ruta V, Chen JY, Lee A, MacKinnon R. The principle of gating charge movement in a voltage-dependent K<sup>+</sup> channel. *Nature*. 2003; 423(6935):42–8. ISI:000182561600033. <https://doi.org/10.1038/nature01581> PMID: 12721619
31. Schmidt T, Ye F, Situ AJ, An W, Ginsberg MH, Ulmer TS. A Conserved Ectodomain-Transmembrane Domain Linker Motif Tunes the Allosteric Regulation of Cell Surface Receptors. *J Biol Chem*. 2016; 291(34):17536–46. WOS:000383241300006. <https://doi.org/10.1074/jbc.M116.733683> PMID: 27365391
32. Todd AE, Orengo CA, Thornton JM. Evolution of function in protein superfamilies, from a structural perspective. *J Mol Biol*. 2001; 307(4):1113–43. WOS:000167977300013. <https://doi.org/10.1006/jmbi.2001.4513> PMID: 11286560
33. Hynes RO. The evolution of metazoan extracellular matrix. *J Cell Biol*. 2012; 196(6):671–9. WOS:000301884900003. <https://doi.org/10.1083/jcb.201109041> PMID: 22431747
34. Groves JD, Tanner MJA. Coexpressed Complementary Fragments Of The Human Red-Cell Anion-Exchanger (Band-3, Ae1) Generate Stilbene Disulfonate-Sensitive Anion Transport. *J Biol Chem*. 1995; 270(16):9097–105. WOS:A1995QU08900011. <https://doi.org/10.1074/jbc.270.16.9097> PMID: 7721823
35. Chothia C, Levitt M, Richardson D. Structure Of Proteins—Packing Of Alpha-Helices And Pleated Sheets. *Proc Natl Acad Sci U S A*. 1977; 74(10):4130–4. WOS:A1977DZ33900005. <https://doi.org/10.1073/pnas.74.10.4130> PMID: 270659
36. Myshkin MY, Paramonov AS, Kulbatskii DS, Lyukmanova EN, Kirpichnikov MP, Shenkarev ZO. "Divide and conquer" approach to the structural studies of multidomain ion channels by the example of isolated voltage sensing domains of human Kv2.1 and Nav1.4 channels. *Russ J Bioorg Chem*. 2017; 43(6):634–43. WOS:000424262900003.

37. Lee SY, Banerjee A, MacKinnon R. Two Separate Interfaces between the Voltage Sensor and Pore Are Required for the Function of Voltage-Dependent K<sup>+</sup> Channels. *PLoS Biol.* 2009; 7(3):676–86. WOS:000265412600023.
38. Trifonov EN. The triplet code from first principles. *J Biomol Struct Dyn.* 2004; 22(1):1–11. WOS:000222865400001. <https://doi.org/10.1080/07391102.2004.10506975> PMID: 15214800
39. Brooks DJ, Fresco JR, Lesk AM, Singh M. Evolution of amino acid frequencies in proteins over deep time: Inferred order of introduction of amino acids into the genetic code. *Mol Biol Evol.* 2002; 19(10):1645–55. WOS:000178497200001. <https://doi.org/10.1093/oxfordjournals.molbev.a003988> PMID: 12270892
40. Brooks DJ, Fresco JR. Increased frequency of cysteine, tyrosine, and phenylalanine residues since the last universal ancestor. *Mol Cell Proteomics.* 2002; 1(2):125–31. WOS:000181515000005. <https://doi.org/10.1074/mcp.m100001-mcp200> PMID: 12096130
41. Wong JT. A co-evolution theory of the genetic code. *Proc Natl Acad Sci U S A.* 1975; 72:1909–12. <https://doi.org/10.1073/pnas.72.5.1909> PMID: 1057181
42. Zuckerkandl E, Derancourt J, Vogel H. Mutational Trends And Random Processes In Evolution Of Informational Macromolecules. *J Mol Biol.* 1971; 59(3):473–+. WOS:A1971K093000006. [https://doi.org/10.1016/0022-2836\(71\)90311-1](https://doi.org/10.1016/0022-2836(71)90311-1) PMID: 5571595
43. Jordan IK, Kondrashov FA, Adzhubei IA, Wolf YI, Koonin EV, Kondrashov AS, et al. A universal trend of amino acid gain and loss in protein evolution. *Nature.* 2005; 433(7026):633–8. WOS:000226862000045. <https://doi.org/10.1038/nature03306> PMID: 15660107
44. Mannige RV, Brooks CL, Shakhnovich EI. A Universal Trend among Proteomes Indicates an Oily Last Common Ancestor. *PLoS Comput Biol.* 2012; 8(12). WOS:000312901500041.
45. Akashi H, Gojobori T. Metabolic efficiency and amino acid composition in the proteomes of *Escherichia coli* and *Bacillus subtilis*. *Proc Natl Acad Sci U S A.* 2002; 99(6):3695–700. WOS:000174511000062. <https://doi.org/10.1073/pnas.062526999> PMID: 11904428
46. vanKlombenburg W, Nilsson I, vonHeijne G, deKruijff B. Anionic phospholipids are determinants of membrane protein topology. *EMBO J.* 1997; 16(14):4261–6. WOS:A1997XM40600011. <https://doi.org/10.1093/emboj/16.14.4261> PMID: 9250669
47. Misawa K, Kamatani N, Kikuno RF. The Universal Trend of Amino Acid Gain-Loss is Caused by CpG Hypermutability. *J Mol Evol.* 2008; 67(4):334–42. WOS:000260282700002. <https://doi.org/10.1007/s00239-008-9141-1> PMID: 18810523
48. Suzek BE, Huang HZ, McGarvey P, Mazumder R, Wu CH. UniRef: comprehensive and non-redundant UniProt reference clusters. *Bioinformatics.* 2007; 23(10):1282–8. WOS:000247348300014. <https://doi.org/10.1093/bioinformatics/btm098> PMID: 17379688
49. Suzek BE, Wang YQ, Huang HZ, McGarvey PB, Wu CH. UniRef clusters: a comprehensive and scalable alternative for improving sequence similarity searches. *Bioinformatics.* 2015; 31(6):926–32. WOS:000352268900017. <https://doi.org/10.1093/bioinformatics/btu739> PMID: 25398609
50. Mirdita M, von den Driesch L, Galiez C, Martin MJ, Soding J, Steinegger M. Uniclust databases of clustered and deeply annotated protein sequences and alignments. *Nucleic Acids Res.* 2017; 45(D1):D170–D6. WOS:000396575500026. <https://doi.org/10.1093/nar/gkw1081> PMID: 27899574